The propagation and linkage of normal faults: Insights from the Strathspey-Brent-Statfjord fault array, northern North Sea

Aileen E. McLeod
Massachusetts Institute of Technology, Earth Resources Laboratory,
42 Carleton Street, Cambridge, MA 02142, USA

Nancye H. Dawers
Tulane University, Department of Geology,
New Orleans, LA 70118, USA

John R. Underhill
University of Edinburgh, Department of Geology and Geophysics,
Grant Institute, Kings Buildings,
West Mains Road, Edinburgh EH9 3JW, UK

Abstract

Through examination of the scaling relations of faults and the use of seismic stratigraphic techniques, we demonstrate how the temporal and spatial evolution of the fault population in a half-graben basin can be accurately reconstructed. The basin bounded by the >>62 km long Strathspey-Brent-Statfjord fault array is located on the western flank of the Late Jurassic age northern North Sea rift basin. Along-strike displacement variations, transverse fault-displacement folds and palaeo- fault tips abandoned in the hangingwall all provide evidence that the fault system comprises a hierarchy of linked palaeo-segments. The displacement variations developed while the fault was in a pre-linkage, multi-segment stage of its growth have not been equilibrated following fault linkage. Using the stratal architecture of syn-rift sediments, we date the main phase of segment linkage as latest Callovian - Middle Oxfordian (10-14 M.yr. after rift initiation). A dense sub-population of faults is mapped in the hangingwall to the Strathspey-Brent-Statfjord fault array. The majority of these faults are short, of low displacement and became inactive within 3-4 M.yr. of the beginning of the extensional event. Subsequently, only the segments of the proto- Strathspey-Brent-Statfjord fault and a conjugate array of antithetic faults located 3.5 km basinward continued to grow to define a graben-like basin geometry. Faults of the antithetic array became inactive approximately 11.5 M.yr. into the rift event, concentrating strain on the linked Strathspey-Brent-Statfjord fault; hence, the basin evolved into a half-graben. As the rift event progressed, strain was localised on a smaller number of active structures with increased rates of displacement. The results of this study suggest that a simple model for the linkage of 2-3 fault segments may not be applicable to a complex multi-segment array.

1 Introduction

Extensional fault systems are dynamic. Faults grow by the processes of radial propagation and the linkage of segments, e.g. Cartwright et al. (1995). As strain increases, an initial fault population of a large number of short, low displacement faults will evolve into a late population comprising a few large fault systems (Cowie, 1998) (Gupta et al., 1998). The temporal and spatial evolution of the fault population within a rift is reflected by changes in the basin topography, and changes in the location, magnitude and rate of generation of accommodation space, e.g. Schlische and Anders (1996),

Dawers and Underhill (2000). Consequently, the distribution and stratal architecture of syn-rift sediments provide a record of coeval tectonic subsidence.

Although numerous studies have shown that tectonic subsidence in the hangingwalls to normal faults is the primary control on the generation of accommodation space in extensional settings, e.g. Leeder and Gawthorpe (1987), Schlische and Olsen (1990), Schlische (1991), Prosser (1993), Anders and Schlische (1994), Gawthorpe et al. (1994), Contreras et al. (1997), patterns of syn-rift sedimentation have been an underutilised tool in the study of normal fault growth. This is largely due to the inherently limited field exposures in exhumed continental rift basins. Even in well exposed basins, like the Miocene Gulf of Suez rift, reconstructions of tectonostratigraphic evolution are generally only possible for local areas and a discrete stage of the rift event, e.g. Armstrong (1997), Gupta et al. (1999). Subsurface studies, in which the entire syn-rift stratal architecture can be resolved, have been restricted by the wide spacing of seismic lines, poor age constraints and the limited area of 3D surveys, e.g. Morley (1999), Contreras et al. (2000), Dawers and Underhill (2000).

In this study we integrate stratigraphic and tectonic evidence to reconstruct the 4-dimensional (temporal and spatial) evolution of a half-graben basin focusing, in particular, on the temporal and spatial distribution of the active fault population, and the timing and rates of fault propagation and linkage processes. This is achieved through the investigation of a unique subsurface dataset that combines 1000 km^2 of 3D seismic coverage (line spacing $\leq$ 25 m) with well data providing biostratigraphically defined ages of syn-rift sediments at a resolution of <3 M.yr. The seismic data encompasses >60 km of the length of the half-graben bounding Strathspey-Brent-Statfjord fault array in the Late Jurassic northern North Sea failed rift system (Fig. 1).

In addition to mapping the distribution and geometries of Late Jurassic faults in the study half-graben, we describe the displacement-length scaling relationships of the structures. Through examination of variations in displacement along the strike of the faults, the mapping of abandoned palaeo-tips and the stratigraphic evidence, the history of segment growth and linkage in the fault population is determined and quantified. From a schematic interpretation of the growth of the Strathspey-Brent-Statfjord fault system, we assess the implications for an improved understanding the distribution and rate of slip during the growth of large normal fault arrays.

2 Northern North Sea Basin

2.1 Structural setting

The Strathspey-Brent-Statfjord fault array is located on the western flank of the northern North Sea rift province (Fig. 1). The northern North Sea basin, one arm of the trilete, failed North Sea rift system, experienced approximately 15 % extension during the Bathonian-Volgian (Yielding, 1990) (Roberts et al., 1993). The majority of the strain is accommodated on large normal fault arrays with displacement maxima typically in excess of 1 km. The fault systems strike N-S in the southern part of the basin and NNE-SSW in the north. Large faults occur at 10-20 km spacing. On a regional scale, the faults describe a graben-like geometry around a central low, the North Viking Graben.

The Strathspey-Brent-Statfjord fault is observed within the area of investigation to be a single throughgoing fault strand with an easterly dip. The southward continuation of the fault, beyond the extent of this study, bounds the eastern margin of the Alwyn North structure (Fig. 1b). The northern tips of the fault overlap with, and are in the footwall of, the Inner Snorre fault segment, part of a major fault array with a total length >90 km and a maximum throw in excess of 3 km.

In the north the Strathspey-Brent-Statfjord fault splits into two strands - the Statfjord (west) and Statfjord East segments - that tip out in the north of the study area (Fig. 1c). Dawers et al. (1999) and Dawers and Underhill (2000) present a detailed examination of the Statfjord East fault segment. They demonstrate that the fault grew from the linkage of a number of shorter fault segments and that the growth of the fault controlled the distribution and character of syn-rift sediments.

2.2 Stratigraphy

Following the cessation of extension in the Early Triassic, the northern North Sea region experienced post-rift thermal subsidence. The area was located in a sand-rich marginal marine setting during the Late Triassic - Early Jurassic (Banks Group) before being rapidly flooded (Steel and Ryseth, 1990). Coincident with the deposition of mud-prone marine deposits (Dunlin Group), the impingement of the Central North Sea Dome was forcing uplift to the south (Underhill

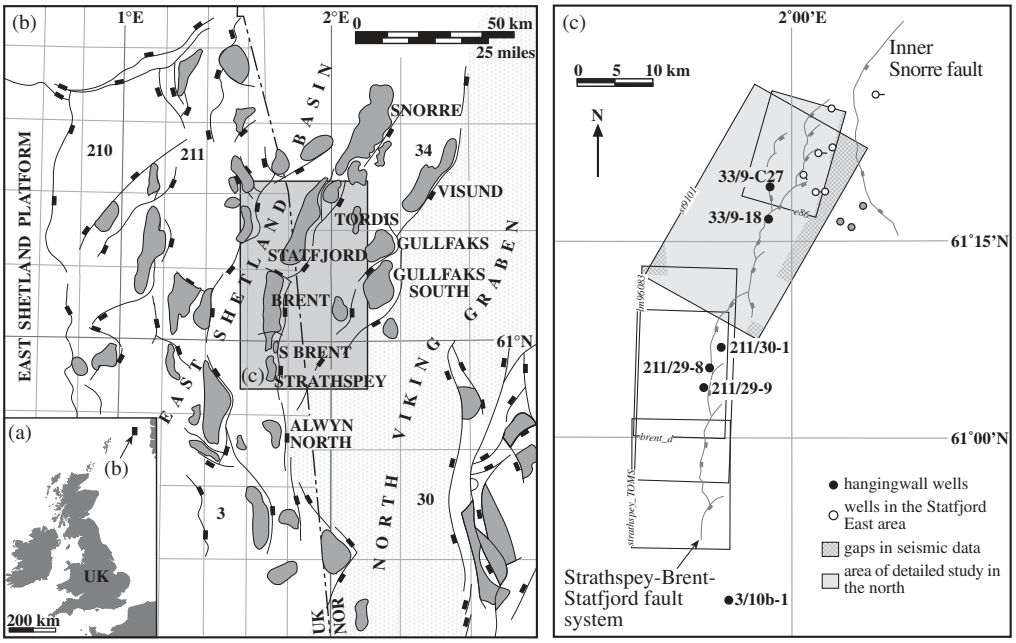

Figure 1: Location of the study area in the East Shetland Basin, northern North Sea. (a) Regional setting; area of (b) illustrated. (b) Principal hydrocarbon fields (shaded dark grey) in the northern North Sea and major normal fault systems; area of (c) illustrated. (c) Map of the study area as defined by the coverage of the five 3D seismic surveys used in this work. Also shown are the locations of hangingwall wells - vertical exploration wells 3/10b-1, 211/29-8, 211/29-9, 211/30-1 and 33/9-18, and deviated well 33/9-C27. Trace of the Strathspey-Brent-Statfjord fault system is shown at the truncation of the top pre-rift reflector in the hangingwall.

and Partington, 1994). This hinterland sourced a major fluvio-deltaic complex (Brent Group) that prograded rapidly north during the Middle Jurassic, e.g. Budding and Inglin (1981), Graue et al. (1987), Helland-Hansen et al. (1992). The Brent delta achieved its maximum northward extent in the Tampen Spur area during the Early Bathonian (Mitchner et al., 1992).

The initiation of extensional tectonics in the northern North Sea during the Middle Jurassic resulted in increased rates of basin subsidence, relative sea level rise and the flooding and retreat of the Brent delta. The Brent Group is a regressive-transgressive package with the youngest lithologies - the heterolithic, sand-rich Tarbert Formation - representing delta retreat during the earliest syn-rift, e.g. Johannessen et al. (1995), Ravnås et al. (1997). Following marine transgression, subsequent syn-rift lithologies of the Humber Group (Heather and Kimmeridge Clay Formations) are typically mud-prone and interpreted as deep marine deposits in a sediment-starved basin, e.g. Rattey and Hayward (1993).

Syn-rift deposits in the Strathspey-Brent-Statfjord area are described in detail by McLeod et al. (in press), and in the Statfjord East area by Dawers et al. (1999), Nøttvedt et al. (2000) and Davies et al. (2000). The distribution and facies mosaic of syn-rift strata were primarily controlled by tectonic activity. The stratigraphic signature of the Tarbert Formation is punctuated transgression, demonstrating that the rate of sediment supply equalled, and locally exceeded, the rate of tectonic subsidence. Although the Humber Group is mud-prone, sand-rich successions are recorded; these are sourced from local footwall degradation (Hesthammer and Fossen, 1999) (McLeod and Underhill, 1999) and, significantly, from erosion of the Snorre structure in the north. Footwall uplift raised the Snorre structure above sea level in the Kimmeridgian-Ryazanian, the erosion of exhumed pre-rift sediments supplying a proximal shoreface and detached turbidite system (Dahl and Solli, 1993). Yielding et al. (1992) have suggested that only the largest (i.e. widest) of the fault blocks were uplifted to, or above, wavebase and, thus, substantially eroded. The footwall of the Strathspey-Brent-Statfjord fault array is considered to be of medium width (for the northern North Sea basin) and to have remained submarine throughout the rift event.

3 Dataset and Methods

3.1 Well data

The hangingwall of the Strathspey-Brent-Statfjord fault system is penetrated by four vertical exploration wells, 211/29-8, 211/29-9, 211/30-1 and 33/9-18, and one deviated production well, 33/9-C27. Some 7 km beyond the southern extent of the seismic coverage, well 3/10b-1 intersects the hangingwall of the Alwyn North structural block (Fig. 1c). All of these wells have cored intervals from the syn-rift, and core samples, detailed biostratigraphy reports and electrical log data from the five wells were used in this study, see also McLeod et al. (in press). In addition, seven wells have been drilled into the hangingwall of the Statfjord East fault segment in the north of the study area. Dawers et al. (1999), Nøttvedt et al. (2000) and Davies et al. (2000) have previously described the log responses and core samples of syn-rift strata in these seven wells. Composite logs and original core reports from these wells were available to this study.

Interpretation of well data identified five key surfaces of litho- and chronostratigraphic significance (Fig. 2): Top Ness Formation, top Tarbert Formation, top Heather Formation, top Kimmeridgian and top Kimmeridge Clay Formation (top syn-rift). Each of these surfaces represents a change in facies and, hence, correlates with a strong seismic reflector. Biostratigraphic dating constrains the top of the Ness Formation to be of latest Bajocian age, top Tarbert Formation to be mid-Bathonian age, top Heather Formation to be top Middle Oxfordian and the top of the Kimmeridge Clay Formation to be Early Ryazanian.

3.2 Seismic data

The area of investigation is defined by the coverage of five migrated 3D seismic surveys with a total areal extent of 965 km^2 (Fig. 1c). The line spacing of these surveys is 12.5-25 m for both W-E/WNW-ESE oriented inlines and N-S/NNE-SSW oriented crosslines. The surveys cover the Strathspey (strathspey-TOMS), Brent (brent-d, lm96083), Statfjord (st9101) and Statfjord East (e86) hydrocarbon fields, which all have oil accumulations in pre-rift strata in the footwall to a Late Jurassic normal fault system.

All the seismic data have a vertical axis in milliseconds two-way-travel time (ms TWT) and it was beyond the scope of this study to depth-convert the data. The results of this study are generally presented with the vertical axis

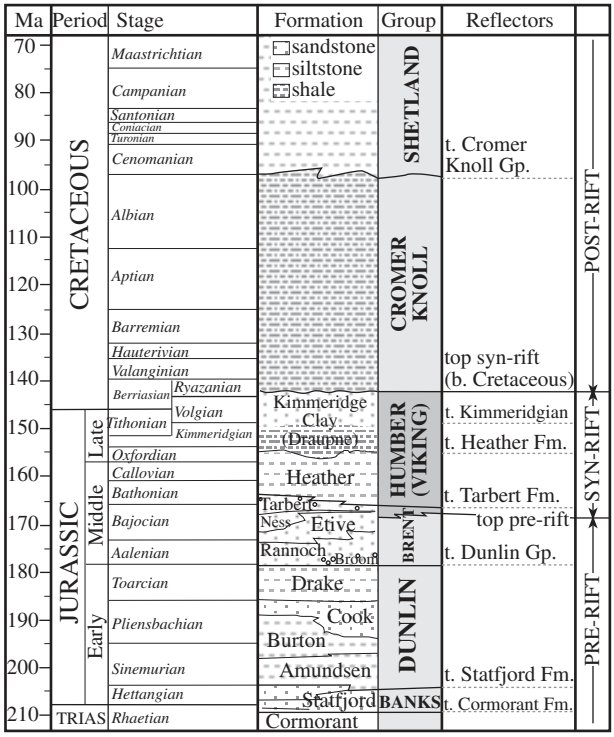

Figure 2: Stratigraphic nomenclature employed in this study, Richards et al. (1993). Also shown are the stratigraphic locations of the key seismic reflectors discussed in this work. Pre-, syn- and post-rift refer to the Late Jurassic extensional event. Based on data from well 33/9-18 (Fig. 11), column modified from Dawers and Underhill (2000) and timescale after Gradstein et al. (1994).

in time; however, a conversion into metres is also presented for key measurements (e.g. the maximum throw on the Strathspey-Brent-Statfjord fault array). This conversion is based on the time-depth relationship in vertical exploration well 211/30-1 located centrally in the study area in the hangingwall basin.

Seismic interpretation was based on correlation with well data. The five key surfaces identified from interpretation of core samples, log signatures and biostratigraphy reports were tied to the seismic data using velocity logs (Fig. 3). The vertical resolution of these reflectors is largely a function of depth (controlling source signal wavelength). The present burial depth of the syn-rift strata of interest is >2.5 km, increasing to in excess of 4.5 km in the south of the study area. Consequently, the vertical resolution of the data (minimum spacing of surfaces for reflection) is estimated to be 10-30 ms TWT. The spacing of seismic lines controls the lateral resolution of reflectors.

Figure 3 is a representative seismic cross section, oriented perpendicular to the strike of the Strathspey-Brent-Statfjord fault array, illustrating the key seismic reflectors and faults mapped in the footwall and hangingwall to the fault system. Sub-parallel, westward dipping reflectors characterise the pre-rift sediments in the footwall to the fault; these reflectors are truncated in the east by the palaeo- footwall scarp. Four pre-rift reflectors were mapped in the footwall (see Fig. 2), including the top pre-rift reflector - a seismic onlap surface. In the hangingwall, the top pre-rift is the deepest reflector mapped. Again this is a marked seismic onlap surface separating the well defined, gently dipping reflectors of the pre-rift from the seismically transparent syn-rift strata. In seismic-well ties, this reflector corresponds with near the top of the Ness Formation (Fig. 2). Within the syn-rift three reflectors were mapped: Top Tarbert Formation, top Heather Formation and top Kimmeridgian. These reflectors, and the strong positive waveform of the top syn-rift (base Cretaceous) reflector, define chronostratigraphically significant packages with markedly different seismic stratigraphic character.

Faults comprising the Strathspey-Brent-Statfjord array were mapped at a line spacing of 62.5-250 m. The crest of the footwall of the fault array is substantially denuded. Thus, in order to measure the throw on the fault, the eroded lithologies had to be reconstructed by extrapolating both the trace of the fault plane and the interpretation of the top pre-rift reflector in the footwall (see Fig. 3). The error in defining the depth of the pre-erosion, palaeo- footwall crest is estimated to be ±25 ms TWT. With the depth axis of the seismic data in time, the dip of the fault is uncertain; hence, throw is measured and consistently used as a proxy for total displacement in this work. For a dip of 60·, the total dip-slip displacement would be 1.15 times the throw; the fault appears constant in dip along-strike.

In addition to the faults of the Strathspey-Brent-Statfjord array, the traces of faults that offset the top pre-rift and intra- syn-rift reflectors were mapped. The displacement-distance profiles of these faults were again constructed from the throw (in ms TWT) of the top pre-rift reflector with a line spacing of throw measurements of 62.5 m.

In general, normal faults with a throw of less than one quarter of the seismic wavelet are difficult to resolve on seismic data. From this, the minimum resolution of faults in this study is a maximum throw of approximately 10 ms TWT. Consequently, the interpretation of seismic data fails to resolve both a population of faults with sub-seismic throws and the tips of faults where displacements are sub-seismic. Previous studies have addressed these limitations by introducing predictions based on the scaling relationships (size-number and displacement-length) of normal fault populations, e.g. Badley et al. (1990), Pickering et al. (1997). Such 'corrections' are not employed in this study. Faults with a maximum throw less than the resolution of the data are ignored. Obviously, without being able to accurately map fault tips and with seismic line spacings of 12.5-25 m, the interpreted fault traces are too short. A realistic reconstruction of the tips of each fault is outwith the scope of this study.

4 Overview of the syn-rift stratigraphic architecture

The half-graben basin bounded by the Strathspey-Brent-Statfjord fault array was sediment-starved during most of the rift event and, consequently, the basin was underfilled. This starvation is evident from the topography of the top syn-rift (base Cretaceous) reflector (Fig. 4) which, barring the effects of post-tectonic compaction and a regional 2-3· southward tilt, equates to the topography (bathymetry) of the basin at the end of rifting. The footwall of the Strathspey-Brent-Statfjord fault system is defined by a linear structural high in the west of the study area, and the hangingwall by a low up to 750 ms TWT (c.1.1 km) deeper than the proximal footwall. The difference in elevation between the footwall crest and the proximal hangingwall represents the remnant, unfilled accommodation space in the basin at the close of the rift phase.

The location of the surface trace of the Strathspey-Brent-Statfjord fault system, and evidence of fault segmentation, can be recognised from examination of the relief of the top syn-rift reflector. The splitting of the fault array into two strands - the Statfjord (west) and Statfjord East segments - in the north of the study area is recorded by the two

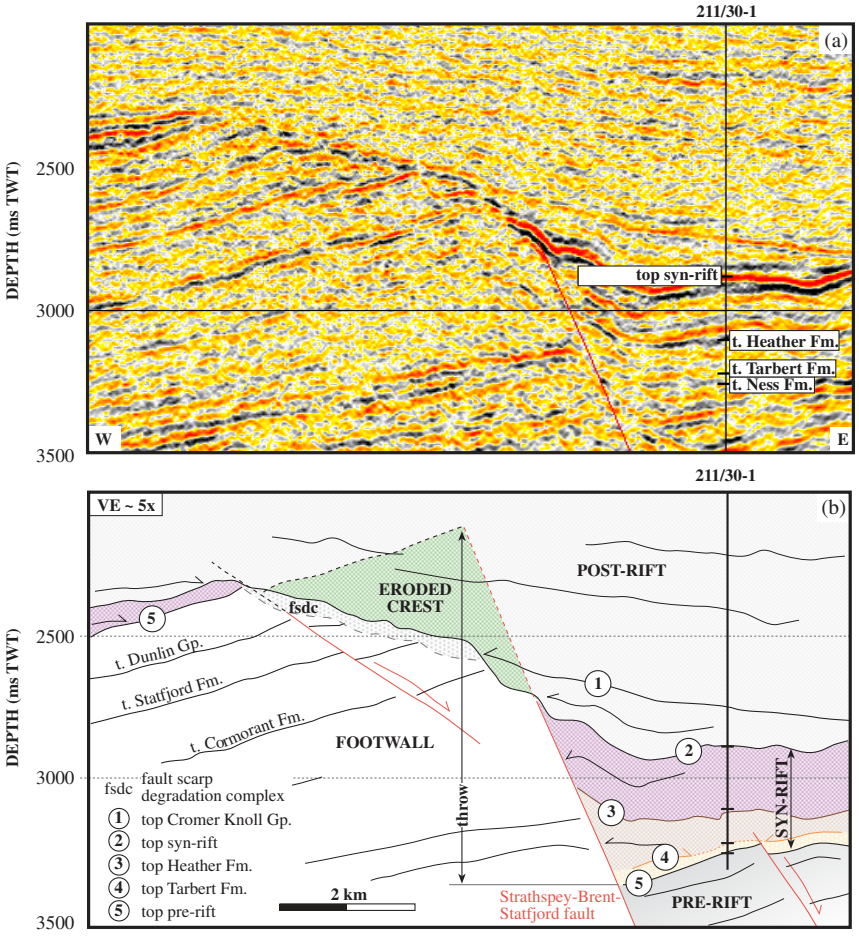

Figure 3: Seismic cross section oriented perpendicular to the strike of the Strathspey-Brent-Statfjord fault array. Key reflectors discussed in this work are shown. The Strathspey-Brent-Statfjord fault is observed to be near planar. (a) Seismic inline 1660 from the Brent (lm96083) survey; line is located on Fig. 7. All seismic lines shown are of the variable amplitude type in which red colours represent positive wavelets and the black colours represent negative wavelets. The seismic data are processed to a normal polarity, zero phase wavelet. (b) Interpretation of seismic inline shown in (a). Reconstruction of the eroded footwall crest is by extrapolation of the top pre-rift and fault reflectors shown (see text for discussion). Vertical exaggeration is approximately five-fold.

footwall highs. To the south, where the fault is a single strand, there is substantial variation in the footwall topography along-strike, even accounting for crestal denudation. Palaeo- structural highs, separated by lows at 7-18 km spacing, are interpreted as the culminations of low amplitude transverse fault-related folds developed in response to differential footwall uplift (Schlische, 1995). Such along-strike variations in fault displacement reflect segmentation; hence, the crestal topography defines the location of an array of shorter palaeo-segments. The major footwall lows (marked A, B and C on Fig. 4) are also the locations of dense populations of normal faults with displacements of up to 250 ms TWT (Fig. 5). These faults offset pre- and syn-rift sediments and segment the footwall into structural blocks (thus defining individual hydrocarbon fields). The faults strike perpendicular to the Strathspey-Brent-Statfjord fault system. They are interpreted as syn-rift accommodation structures developed in response to local extensional stresses in the footwall due to the steep displacement gradients formed at the tips of palaeo-fault segments as the faults interacted and linked.

The effects of along-strike variations in fault displacement are also demonstrated by the topography of the top pre-rift reflector in the hangingwall (Fig. 5). This surface is observed to dip both southward, due to post-tectonic tilting, and westward into the fault, as would be predicted by conventional half-graben models. Overprinted on the southwesterly dip, however, are a series of folds (or depocentres) with hingelines oriented perpendicular to and plunging towards the fault. Folds are observed on two scales (see Fig. 5): Larger structures of up to 600 ms TWT amplitude and 4-13 km width, within the bounds of which are smaller folds of <150 ms TWT amplitude and 1-3 km width. The anticlinal intra-basin highs bounding the larger folds (marked A, B and C on Fig. 5) correspond with the locations of major synclinal lows on the footwall (A, B and C on Fig. 4). Folding of the top pre-rift reflector is interpreted to be a consequence of differential displacement - analogous to the transverse fault-displacement folds of Schlische (1995). Thus these folds preserve a record of the along-strike displacement variations of shorter palaeo-segments developed prior to fault linkage. Hangingwall folds are of higher amplitude than those in the footwall due to the distribution, in terms of uplift and downthrow, of coseismic slip, e.g. Stein and Barrientos (1985). These geometric observations indicate that palaeo- fault segments of 1-3 km length linked to form longer arrays of 4-13 km length before the fully linked, throughgoing strand was established.

These conclusions are supported by the seismic stratigraphic architecture of the basin. A fault parallel cross section proximal to the Statfjord structure is presented in Fig. 6. Thickness variations and onlap geometries within the syn-rift demonstrate that the smallest folds were developed earliest in the rift event, and that the accommodation space was filled with sediments before the larger structures evolved. This is compatible with the observation that small faults grow into large faults through segment linkage, e.g. Cartwright et al. (1995), Cowie (1998). Assuming sediment supply kept pace with subsidence, the timing of fault growth is dated by these sediments infilling the accommodation space (discussed later in this paper). Although this half-graben is recognised to be underfilled in terms of the entire rift event, studies of the early syn-rift sediments (Davies et al., 2000) (McLeod et al., in press) demonstrate that during the 'rift initiation' phase of extension, after Prosser (1993), the rate of sediment supply was equal to, or exceeded, the rate of tectonic subsidence. This depositional motif of high rates of sediment supply early in the extensional event followed by flooding and basin starvation is typical of many rift basins (Lambaise, 1990) (Schlische and Olsen, 1990).

5 The fault population

Two sub-populations of normal faults are described in the study area, distinguished by the size of the faults and the period of time, during the rift phase, when they were active. The two sub-populations are described separately below.

5.1 Character of the SBS fault

5.1.1 Location and form of the fault segments

The sub-population of faults described in this section comprises all the structures related to the lateral propagation and growth of the largest single fault in the study area - the Strathspey-Brent-Statfjord fault. This sub-population can be divided into (1) the main fault itself, and (2) a group of ten splays from this fault, located at between 5-13 km spacing in the immediate hangingwall to the Strathspey-Brent-Statfjord fault (Fig. 7).

The Strathspey-Brent-Statfjord fault is the most significant fault in the study area in terms of length and displacement. This structure is a continuous, thoroughgoing normal fault strand with a maximum displacement in excess of 2 km. The southern tip of the fault is not covered by the available seismic data; hence, the total length of the fault in the study area is >>62 km. As described earlier, the fault splits into two segments in the north - the Statfjord (west)

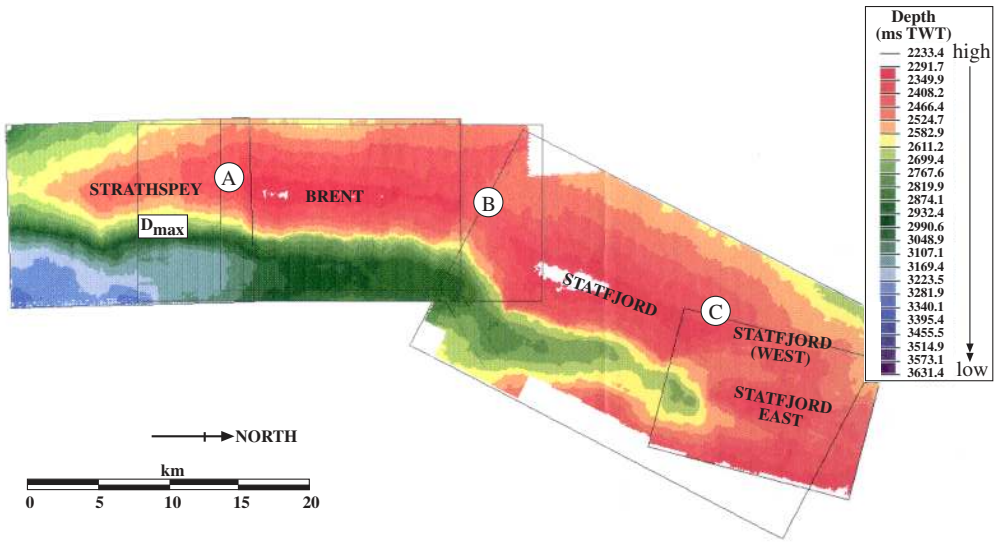

Figure 4: Map of the depth (in ms TWT) to the top syn-rift (base Cretaceous) reflector. The topography on this surface equates to the basin floor topography at the end of the rift event (barring the effects of post-tectonic compaction and tilting). A, B and C are structural lows on the footwall.

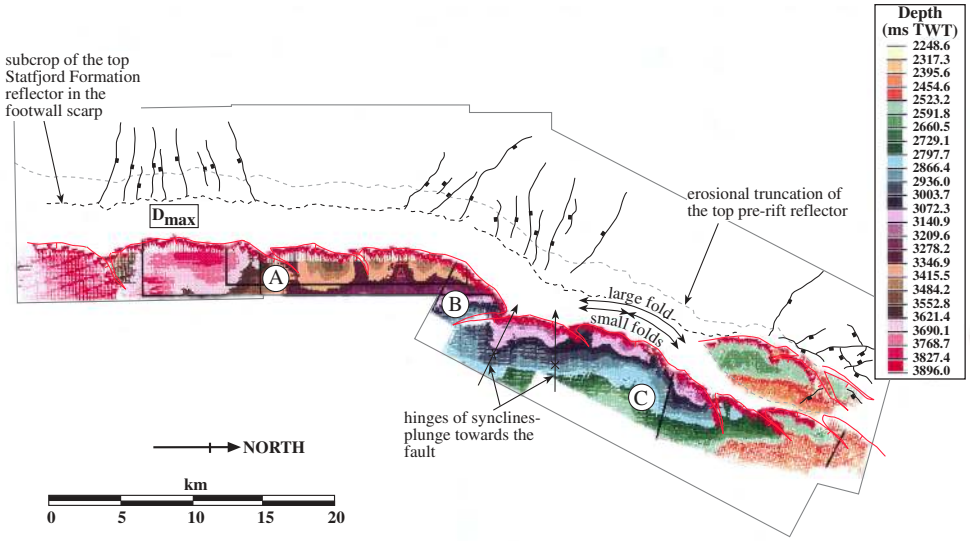

Figure 5: Map of the depth (in ms TWT) to the top pre-rift reflector in the hangingwall to the Strathspey-Brent-Statfjord fault array. A hierarchy of fault proximal depocentres is defined. These folds are interpreted as transverse fault-displacement anticlines, after Schlische (1995), and, hence, locate palaeo- fault segments. A, B and C are the locations of intra-basin highs in the hangingwall; these points correspond with the footwall lows shown in Fig. 4. Faults in the footwall are mapped at the downthrown contact with the top Statfjord Formation reflector. These faults have maximum displacements of <250 ms TWT.

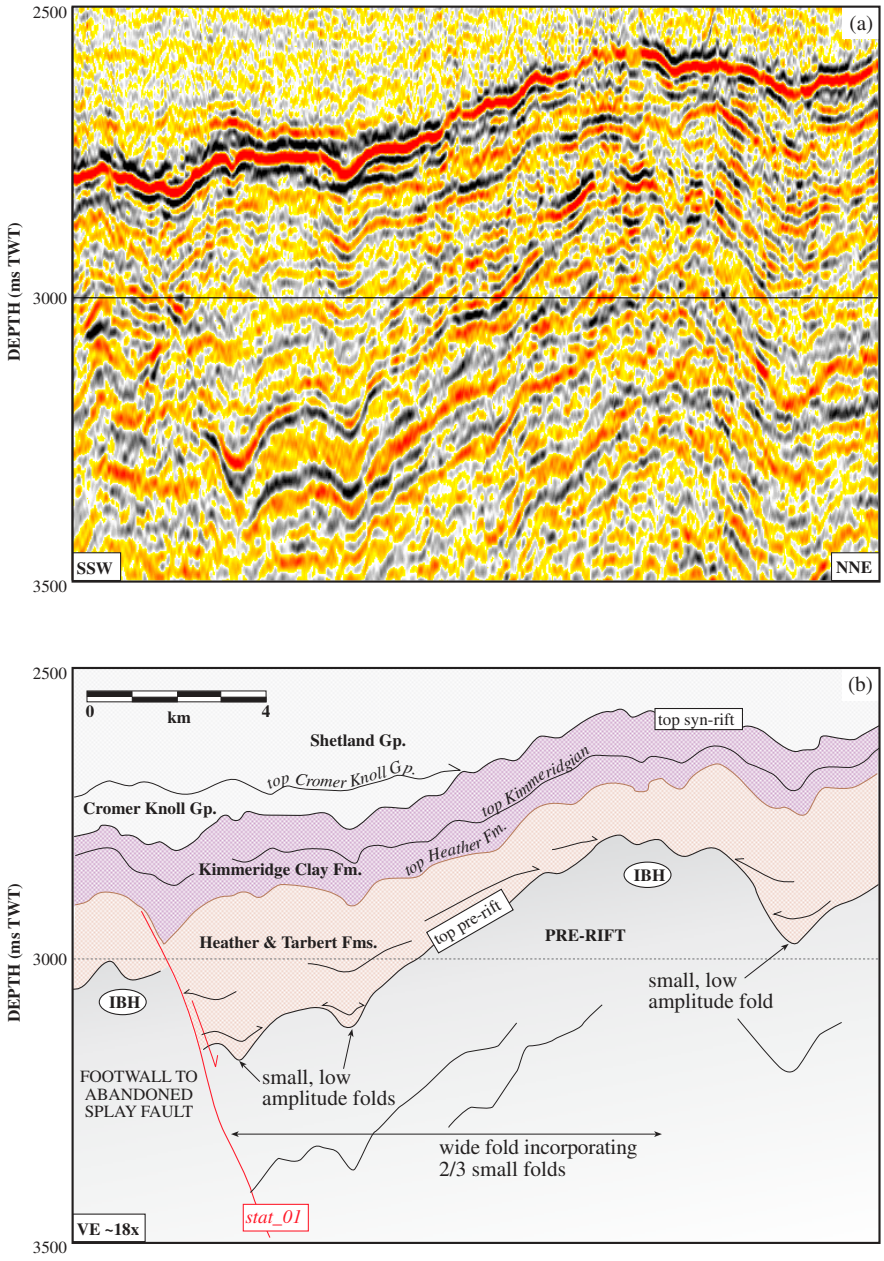

Figure 6: The geometry of transverse fault-displacement folds in the hangingwall to the Strathspey-Brent-Statfjord fault array. Folds are observed to be of highest amplitude at top pre-rift level. Folds persist into the lower post-rift due to differential sediment compaction and basin starvation. (a) Seismic crossline 430 from the Statfjord (st9101) survey, proximal and strike parallel to the Strathspey-Brent-Statfjord fault; line is located on Fig. 7. (b) Interpretation of the seismic line shown in (a). IBH = intra-basin high. The fault shown is an abandoned tip. Vertical exaggeration is approximately eighteen-fold.

fault and the Statfjord East fault. The Statfjord (west) segment tips out within the area of the seismic coverage, the Statfjord East fault a further c.2 km to the north, see Dawers and Underhill (2000).

The cross-sectional geometry of the fault plane is, typically, near planar (Fig. 3). Curvature observed in some areas, particularly in the Statfjord (st9101) survey, suggests that some structures may be listric in form at depth. The two northern segments of the Strathspey-Brent-Statfjord fault are also observed to be near planar in across strike section (Fig. 8). The two seismic cross sections in Figs. 3 and 8 demonstrate the footwall of the Strathspey-Brent-Statfjord fault to be substantially denuded along its entire length and the crest to be erosionally backstepped by 2-3 km.

The fault can be mapped along the entire N-S length of the study area, striking N-S in the south (Strathspey and Brent areas) and rotating to a NNE-SSW trend in the north (Statfjord area). The change in the strike of the fault corresponds with an c.4 km eastward step of the fault trace (annotated on Fig. 7). The fault trace is not linear in map view, but rather has a multiple cuspate form. Low amplitude arcs come to apices spaced at 4-13 km (see Fig. 7). It is at the apices of some of these cusps that the ten fault splays intersect with the Strathspey-Brent-Statfjord fault. The splays arc out into the hangingwall basin from the main fault with generally a NE-SW strike. They are up to 3 km in length, with a maximum throw of up to 300 ms TWT (c.450 m; strath-01). The points of intersection of the splays correspond with the locations of structural lows in the footwall (Fig. 4).

Displacement-distance profiles for the splays, based on the offset of the top pre-rift reflector, are near linear in form (Fig. 9). Maximum displacement occurs at the western end of the faults where they intersect with the Strathspey-Brent-Statfjord fault. Displacement decreases along the length of the splays, typically to zero within 3 km. Such displacement-distance profiles are incompatible with the triangular or flat-topped profiles described from single, isolated normal faults, e.g. Peacock and Sanderson (1991), Peacock and Sanderson (1994), Dawers et al. (1993), Childs et al. (1995) and predicted by fault growth models, e.g. Cowie and Scholz (1992). The faults rather have the form of just one half (or less) of a fault, i.e. a fault tip.

In seismic cross section perpendicular to strike, the vertical form of the splay faults is near planar (Fig. 8). Although demonstrated in map view to intersect with the Strathspey-Brent-Statfjord fault, splay faults are located in the downthrown hangingwall to the half-graben bounding fault. The vertical trace of the splays cannot be mapped through the entire syn-rift, indeed the splays rarely offset the top of the Heather Formation although this formation is substantially thickened in the hangingwalls. Hence, these small faults are concluded to have only been active early in the rift event, between latest Bajocian - Middle Oxfordian (see Figs. 7 and 8, and later discussion).

The observations of fault location and form presented above suggest that the splay faults represent the palaeo-tips of normal faults, which, when two overlapping segments 'hard-linked', were abandoned in the hangingwall to the new longer fault, i.e. 'footwall breached relays' of Trudgill and Cartwright (1994). This is compatible with the stratigraphic evidence, see also McLeod et al. (in press), and with the interpretation of these structures in the Statfjord East area by Dawers et al. (1999) and Dawers and Underhill (2000). The implication of this conclusion is that the Strathspey-Brent-Statfjord fault grew from the linkage of at least eleven shorter segments of 7-15 km length, whose location can be determined from the 'cusp-shaped' form of the fault trace, the abandoned tips in the hangingwall and structural lows on the footwall. Hence, the main fault and the splay faults can be considered as part of an integrated fault system associated with the growth of the Strathspey-Brent-Statfjord fault.

5.1.2 Observations from displacement-distance profiles

The conclusions presented above are supported by observations from the displacement-distance profiles of faults forming the Strathspey-Brent-Statfjord fault system. Figure 9 shows the individual profiles for the main fault and each of the ten splay faults, plotted along a 65 km long horizontal axis parallel to strike (i.e. N-S oriented in the south, NNE-SSW in the north; see Fig. 7). These profiles measure the throw (in ms TWT) of the top pre-rift reflector, as illustrated in Fig. 3.

The displacement-distance profile of the Strathspey-Brent-Statfjord fault (including the summed displacements of the Statfjord (west) and Statfjord East fault segments) has a truncated flat-top shape with a linear tip gradient (Fig. 9). Maximum displacement of 1552 ms TWT (2326 m) is located 12.5 km from the southern extent of the study area (Fig. 7). For c.48 km from this southern margin the total displacement on the fault is >750 ms TWT (>1.2 km). Two kilometres north of where the fault splits into two strands, the displacement begins a steep decline to zero within 10 km. A similar tip profile is assumed in the south. This profile shape, and the distribution of the displacement over multiple strands at the tips, are compatible with previous descriptions of large, isolated normal faults, e.g. Ebinger et al. (1999), Morley (1999).

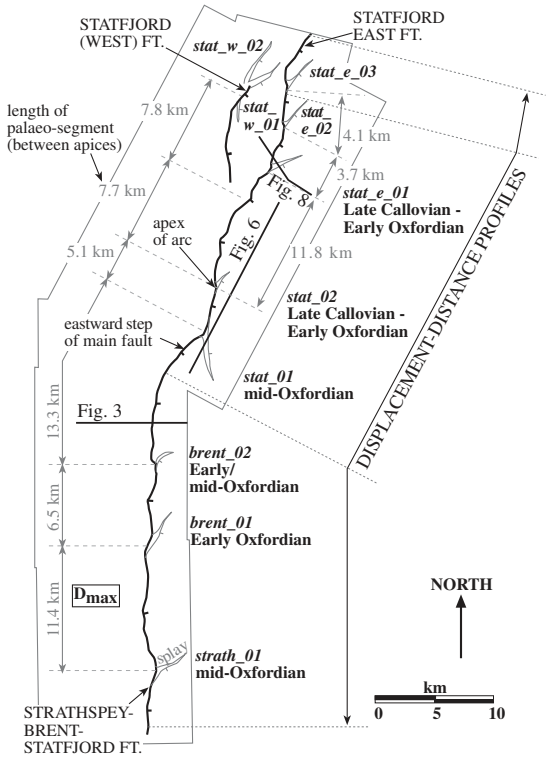

Figure 7: Map of the fault population associated with the Strathspey-Brent-Statfjord fault system. The throughgoing half-graben bounding Strathspey-Brent-Statfjord fault strand is shown in black (mapped at the downthrown contact with the top pre-rift reflector). Ten splays from this fault are shown in grey and named. Ages refer to the time that significant activity ceased on these faults (from seismic stratigraphic evidence, see text). Also shown are the locations of the seismic lines in Figs. 3, 6 and 8 and the strike orientation of the displacement-distance profile in Fig. 9.

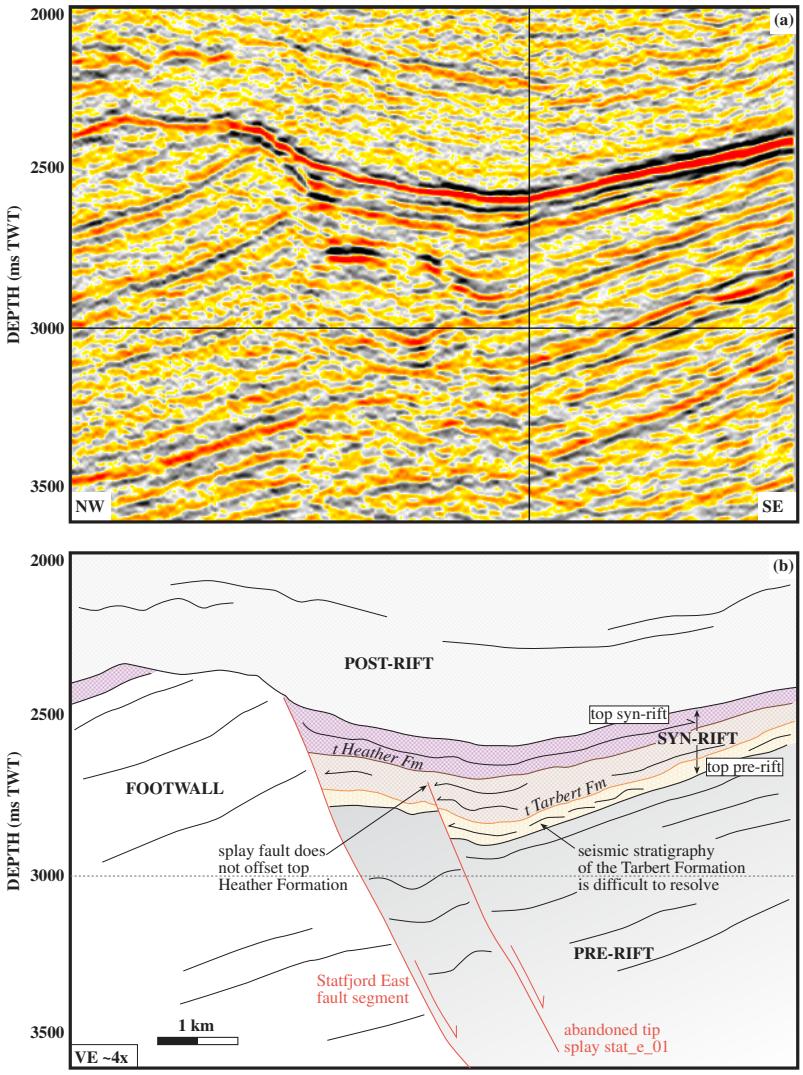

Figure 8: Seismic cross section oriented perpendicular to the strike of the Strathspey-Brent-Statfjord fault array (Statfjord East fault segment) and an abandoned palaeo-tip (stat-e-01). (a) Seismic traverse from the Statfjord East (e86) survey; line is located on Fig. 7. (b) Interpretation of the seismic traverse shown in (a). Vertical exaggeration is approximately four-fold.

Although an overall flat-topped profile shape is suggested, the displacement-distance profile of the Strathspey-Brent-Statfjord fault is not smooth, rather it is extremely serrated with vertical variations of up to 422 ms TWT (638 m). These displacement variations are not random but define a pattern with displacement minima of comparable magnitude occurring every 3-6 km. It is noted that these displacement minima on the main fault system may represent zones where displacement is distributed across numerous small faults that cannot be resolved on the seismic dataset. Along-strike displacement variations are shown in greater detail for the central (10-30 km distance on Fig. 9) part of the fault in Fig. 10a. Displacement minima are used as boundaries to define constituent, first-order units (Fig. 10a). The minimum values are between 102-422 ms TWT (153-638 m) less than the local maxima. Maxima tend to be skewed 1-3 km from the centre of units. A further two or three minima and maxima at 0.5-3 km spacing can be recognised within each unit, typically representing local displacement variations of <150 ms TWT (<225 m). It is observed that some of the minima bounding first-order units correlate with the locations of intra-basin highs in the hangingwall and abandoned palaeo-tips (Fig. 9). The second-order units correspond with the small folds of the top pre-rift reflector (Fig. 5). Hence, in addition to the 7-15 km long segments previously identified from the locations of abandoned tips (and supported by these observations), a number of shorter segments of 0.5-3 km length, from earlier still in the rift history, are recognised.

Significantly, and in contrast to the predictions of the conceptual model of Cartwright et al. (1995), the along-strike displacement variations of these shorter segments have not been completely equilibrated during continued fault growth after linkage. Rather these displacement variations appear to have been preserved, as a record of the geometry of the earlier fault population, in the displacement-distance profile of the linked system.

The serrations in the displacement-distance profile of the Strathspey-Brent-Statfjord fault, between 3.5-49 km along-strike, were used to estimate the minimum values of length and maximum displacement of earlier segments (see Fig. 10a). These are minimum estimates as segments may not link tip to tip but may instead first grow into an overlapping geometry. Palaeo-tips abandoned in the hangingwall suggest that some of the >3 km long segments may have been up to 4 km longer pre-linkage and had maximum displacements up to 300 ms TWT (c.450 m) greater.

The displacement and length data interpreted for these palaeo-segments are shown in Fig. 10b as a plot of the minimum length against the displacement anomaly (as preserved on the displacement-distance profile of the linked fault). Also shown for comparison on Fig. 10b is the range of maximum displacement/throw and length data for the global dataset, as discussed in Schlische et al. (1996). Note that both the length and maximum displacement of these faults are minimum measures and that maximum displacements are measured in TWT. The data are presented as two groups in Fig. 10b. The first represents the largest palaeo-segments, i.e. the first-order units described in Fig. 10a, of minimum length >3 km. These are commonly associated with the abandoned tips; hence, the segments are confidently interpreted to represent unique structures. The second group is the second-order units described in Fig. 10a, bounded by local displacement minima within the larger units. The minimum length of these faults is between 0.5-4 km, and the folding of the top pre-rift reflector supports their origin as unique faults. The whole dataset shows a distinct trend sub-parallel to, and clustering around, the trend of the global dataset.

These observations are somewhat surprising. They indicate that displacement variations along the length of a normal fault system developed while the fault was in a pre-linkage, multi-segment stage of its growth are not lost, and indeed show little equilibration at all, as the fault links and grows. The reason for the lack of equilibration of displacement after linkage to support the longer fault length is unclear. A preliminary interpretation maybe that it reflects the immaturity of the fault system, that it was 'switched off' while in the process of linkage and never had the opportunity to accumulate vertical displacement to mirror its along-strike length. This conclusion is, in part, supported by the observation that the maximum displacement of the whole fault system (c.2.3 km) is lower than would be predicted for its length (for faults in the Basin and Range, Dmax = 0.03L; Dawers (1997)). The implications of these observations and conclusions for understanding the distribution and rate of displacement on this fault during growth are considered below.

5.1.3 On the timing of segment linkage

The observations presented above demonstrate that the Strathspey-Brent-Statfjord fault grew by a mappable process of segment linkage. However, in order to appreciate the implications of constraining fault growth patterns for understanding both the topographic evolution of the basin and sediment dynamics, a temporal framework is required. The timing of activity on the main fault and the abandoned splays can only be constrained through examination of the seismic stratigraphic architecture of syn-rift deposits. Specifically, we recognise thickening of sediments into active faults and sedimentation across the trace of inactive structures. Using sedimentation patterns to date coeval fault

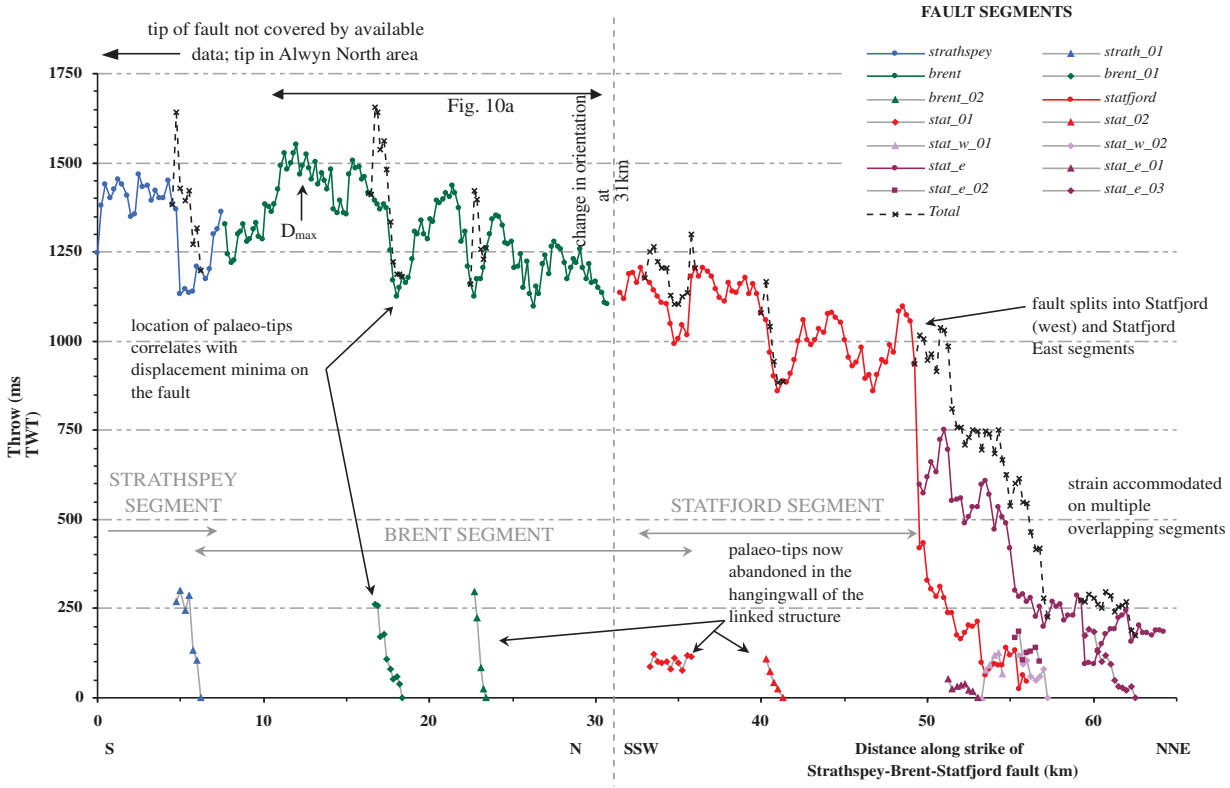

Figure 9: Displacement-distance profiles for the Strathspey-Brent-Statfjord fault and the splay faults. Horizontal distance is parallel to the strike of the half-graben bounding fault (N-S in the south, rotating to NNE-SSW in the north, see Fig. 7). Vertical scale is throw (in ms TWT) of the top pre-rift reflector (Fig. 3). Maximum throw of 1552 ms TWT equates to c.2.3 km.

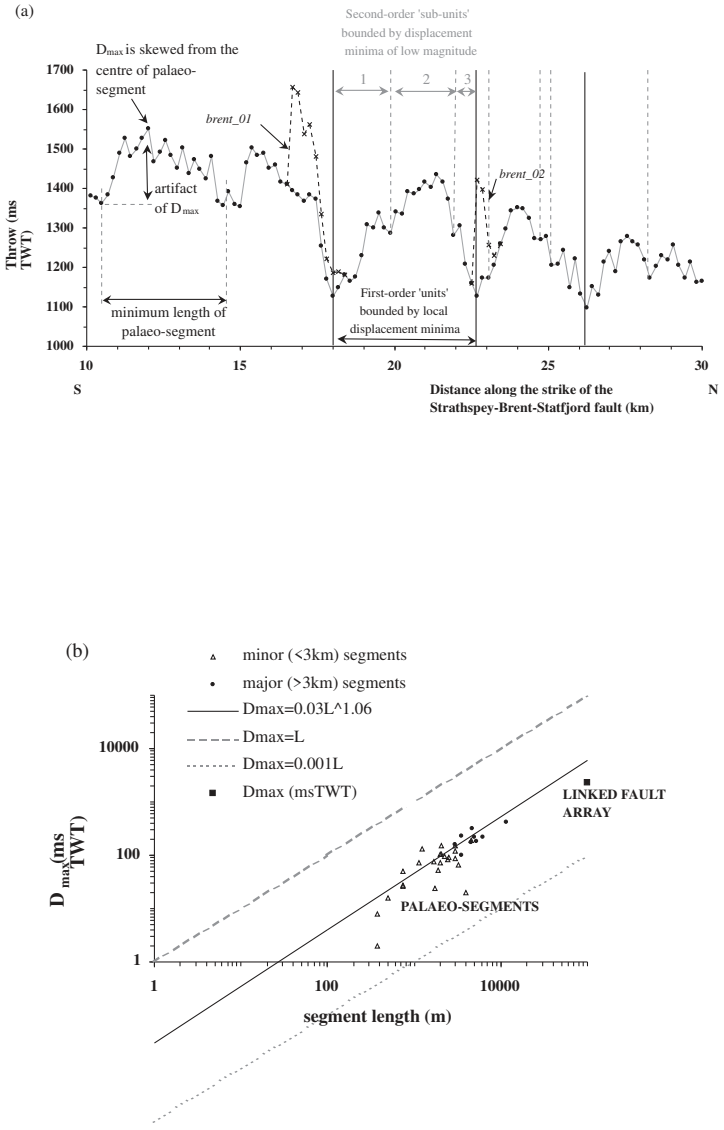

Figure 10: Displacement variations along the strike of the Strathspey-Brent-Statfjord fault array. (a) Expansion of the displacement-distance profile of the fault for 10-30 km along-strike (Fig. 9). The first-order units shown are bounded by significant local displacement minima that correspond with the locations of abandoned fault tips (e.g. brent-01, brent-02). Second-order sub-units are bounded by displacement minima of lower magnitude. The correlation of these sub-units with the small depocentres on the top pre-rift reflector (Fig. 5) supports the interpretation that these sub-units are the remnant displacement-distance profiles of palaeo- fault segments. (b) Plot of minimum segment length against displacement anomaly (as defined in (a)) for 33 first- and second-order palaeo-segments identified between 3.5-49 km along the strike of the Strathspey-Brent-Statfjord fault. Note that both the length and maximum displacement of these palaeo-segments are under-represented as the contribution of abandoned tips is not taken into account (see text). The conversion of throw (in ms TWT) to displacement (in m) would increase values by around a third.

activity requires that the rate of sediment supply kept pace with the rate of tectonic subsidence. Examination of the sedimentary history of the half-graben bounded by the Strathspey-Brent-Statfjord fault array demonstrates that the rate of sediment supply was near equal to the rate of tectonic subsidence during the earliest stages of rifting, but that tectonic subsidence greatly outpaced sediment supply during the rift climax (McLeod et al., in press).

All of the lithostratigraphic units described within the syn-rift (Tarbert, Heather and Kimmeridge Clay Formations) are observed to thicken into the Strathspey-Brent-Statfjord fault (Fig. 3). Hence, the fault was active throughout the period of extension (latest Bajocian - Ryazanian), approximately 30 M.yr. In order to achieve 2.3 km of displacement, this would equate to an average displacement rate of 76.7 mm/ka. However, the magnitude of syn-rift thickening into the fault is extremely variable along the length of the structure and for different intervals within the syn-rift (Fig. 6). Assuming that sediment supply was equal along the fault at any given time, this suggests that the rate of displacement and, hence, the volume of accommodation space created in the hangingwall to this fault were temporally and spatially variable throughout the rift event, as would be predicted by a model of fault growth by segment linkage, e.g. Cowie (1998), Gupta and Scholz (2000).

The magnitude of along-strike variations in the thickness of the syn-rift succession is demonstrated by comparison of Figs. 3 and 8. The fault perpendicular cross section shown in Fig. 3 dissects one of the major depocentres defined in Fig. 5; in Fig. 3 the syn-rift is c.500 ms TWT thick and all the packages thicken into the fault. In the study area, the syn-rift achieves a maximum thickness of c.700 ms TWT in the proximal hangingwall to the position of maximum displacement on the fault system. In contrast, Fig. 8 shows a section across the Statfjord East fault segment in the north of the area where a major splay fault is located in the hangingwall to the main fault. The proximal syn-rift in this area is substantially thinner; in the hangingwall to the splay fault the syn-rift is c.350 ms TWT thick. In addition, the Tarbert and early Heather Formations thicken into both the splay fault and the main fault, and the late Heather and Kimmeridge Clay Formations only thicken into the Stafjord East fault. Thus, the splay fault and the main fault were both active early in the syn-rift but, following fault linkage, the main fault was the only active fault. Across the study area, places where the syn-rift is observed to be thin and to have less pronounced thickening into the Strathspey-Brent-Statfjord fault correspond with local displacement minima and the locations of abandoned splays. Using these observations and stratigraphic dating, it is possible to determine when splay faults became inactive, i.e. linkage occurred (annotated on Fig. 7), and to map the growth of the Strathspey-Brent-Statfjord fault.

Recognising that the main period of segment linkage of the Strathspey-Brent-Statfjord fault was during the latest Callovian - Middle Oxfordian, it is possible to assess general changes in the magnitude of slip rates on the fault. For example, prior to linkage the 12 km long palaeo-segment bounded by the splay fault brent-01 probably had a maximum displacement of 420 ms TWT (630 m) (including the abandoned tip, Fig. 10). Splay fault brent-01 became inactive during the Early Oxfordian, thus the maximum pre-linkage displacement rate was c.55 mm/ka. However, after linkage the fault at this location accumulated another 1132 ms TWT (1.7 km) of displacement before becoming inactive in the Ryazanian. Consequently, average displacement rates were c.92 mm/ka. This increase in the average rate of displacement marks the transition from the 'rift initiation' to 'rift climax' phases of extension, after Prosser (1993). This transition has previously been discussed by Gupta et al. (1998) and related to interactions between fault segments that begin just prior to segment linkage.

5.2 Faults in the hangingwall of the SBS fault

A second sub-population of normal faults was identified by seismic interpretation in the northern part of the study area (see Fig. 1c). Faults were mapped in the hangingwall of the Strathspey-Brent-Statfjord fault where they offset the top pre-rift reflector (Fig. 11). A map of the sub-population of faults is shown in Fig. 12.

Of a total of 53 seismically resolvable normal faults identified, 22 are antithetic to the Strathspey-Brent-Statfjord fault array and 31 are synthetic. Synthetic faults are distributed within 1-3 km of the main fault system and tend to define two sub-parallel trends approximately 0.75 km apart. Antithetic faults, in contrast, form a distinct, multi-segment single trend some 3.5 km east of the half-graben bounding fault. It is noted that few faults are mapped within 1.5 km of the main fault system. The overall geometry of the faults in the hangingwall is graben-like (Fig. 11), with the graben axis c.3 km to the east of, and striking parallel to, the Strathspey-Brent-Statfjord fault.

The sub-population of hangingwall faults range in (mappable) length from 125 m to >5 km and all strike near parallel to the proximal Strathspey-Brent-Statfjord fault. The maximum displacement on the 53 faults is 12-210 ms TWT (15-315 m). Again throw is used as a proxy for displacement. Displacement-distance profiles of 39 faults from the sub-population (numbered in Fig. 12), demonstrate that the majority have a maximum displacement of <50 ms

TWT and are <2 km in length (Fig. 13a). Of these 39 faults, only 5 have a maximum displacement in excess of 75 ms TWT. These 5 faults (faults 7, 16, 22, 24 and 30) are the longest segments of the antithetic fault trend located 3.5 km east of the main fault (Fig. 12).

The resolution of the seismic data, the size of the faults and the sampling interval (every 125 m) do not permit detailed analysis of the displacement-distance profiles of these faults. However, general observations of skewing of the profiles of overlapping segments (faults 16 and 22; Fig. 13a) and a distribution of displacement between faults with two overlapping strands (faults 22 and 24; Fig. 13a) are made. In addition, the ratio of maximum displacement to length of the 39 faults is demonstrated to show reasonable correlation over two orders of magnitude (Fig. 13b), with a best-fit linear relationship for the sub-population of Dmax = 0.0357L (correlation coefficient, $R^2 = 0.663$).

Similar to the work presented in the preceding section, the timing of activity on these faults can only be determined indirectly, i.e. by seismic stratigraphic techniques. Figure 11 shows a WNW-ESE oriented seismic inline from the Statfjord (st9101) survey that crosses the path of vertical exploration well 33/9-18. The line drawing interpretation in Fig. 11b shows biostratigraphic picks in well 33/9-18, and also the interpretation of antithetic faults 24 and 30 and synthetic fault 28. The two central faults 28 and 30 offset the top Tarbert Formation reflector and the formation thickens across the faults. The vertical traces of these faults, however, terminate in the very earliest Heather Formation and the faults clearly do not offset the top Heather Formation reflector. Biostratigraphic dating of the Tarbert and Heather Formations in 33/9-18 indicates that the two faults were active only during the latest Bajocian - Middle Bathonian (3-4 M.yr.). In contrast, the antithetic fault 24 appears to have had a longer period of activity. Not only does the Tarbert Formation thicken into this fault, but the Heather Formation also thickens. The fault does not offset the top of the Heather Formation, and thickening in the overlying Kimmeridge Clay Formation is attributed to the effects of differential compaction. Allowing for basin starvation, the duration of activity on this fault is interpreted as latest Bajocian - ?earliest Oxfordian (11.5 M.yr.).

The timing of activity of the hangingwall faults can be related to the size of the fault. The shorter faults (<3 km length) became inactive in the Middle - Late Bathonian. This includes all of the faults synthetic to the Strathspey-Brent-Statfjord fault, and some of the antithetic structures. The antithetic faults that continued to accumulate significant displacement after the Late Bathonian were those faults forming the main antithetic fault trend located 3.5 km east of the half-graben bounding fault system (i.e. faults 7, 16, 22, 24, 30, 32 and 36). The maximum displacement rates of the faults located in the hangingwall to the Strathspey-Brent-Statfjord fault are <30 mm/ka.

5.2.1 On the growth of the hangingwall fault population

The observations presented above demonstrate that early in the rift event a large sub-population of normal faults nucleated and grew in the hangingwall of the developing Strathspey-Brent-Statfjord fault. Of this sub-population, the majority of faults became inactive after 3-4 M.yr. This majority comprised faults <3 km in length, mainly synthetic to the main trend and located within 3 km of that structure. The minority of faults that continued to grow formed a multi-segmented antithetic fault array, located 3.5 km east of the main fault. Faults of the antithetic trend also became inactive, after 11.5 M.yr., when segment lengths were up to 5 km.

Figure 14 shows a 5.6 km wide, WNW-ESE oriented seismic inline and interpretation of the hangingwall basin. This view emphasises the graben-like form of the fault population and the dominance of the antithetic faults in the basin. This line also shows that the main antithetic fault and the Strathspey-Brent-Statfjord fault meet at depth. In the study area, the depth at which the two faults meet is consistently in the range 900-1000 ms TWT. The geometry of this sub-basin is comparable with the geometry of most other documented half-graben type continental rift basins. That is, an asymmetric basin bounded by a major normal fault system with several kilometres of displacement and segmented along-strike. The hangingwall basin is commonly observed to be dissected by a major antithetic structure, e.g. Roberts and Jackson (1991), Hayward and Ebinger (1996), Morley (1999). The growth of the antithetic structure is restricted by the inability of active faults to cross, e.g. Jackson and McKenzie (1983). This study supports the simple model of rifting, summarised by Scholz and Contreras (1998), in which the rift is initially symmetric, with the formation of conjugate fault sets, but faults are locked by intersection at depth. The fault that reaches the intersection point first will dictate which of the two continues to grow. In this fault system, the Strathspey-Brent-Statfjord fault is, thus, considered to have grown most rapidly and 'switched off' the antithetic faults by locking at depth.

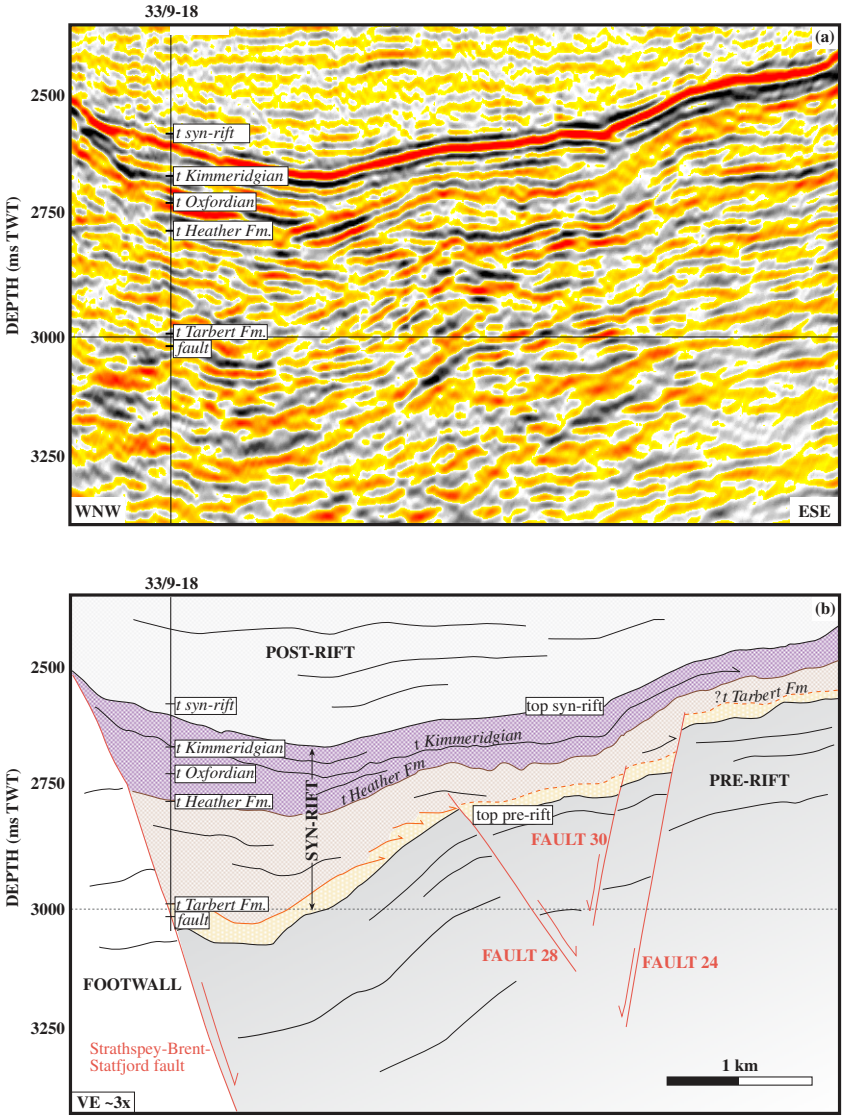

Figure 11: Interpretation of faults in the hangingwall to the Strathspey-Brent-Statfjord fault array. (a) Seismic inline 700 from the Statfjord (st9101) survey; line is located on Fig. 12. (b) Interpretation of the seismic inline shown in (a). This line intersects the path of well 33/9-18, and lithostratigraphic and chronostratigraphic picks in this well are used to determine the timing of activity on the faults. See text for discussion. Vertical exaggeration is approximately three-fold.

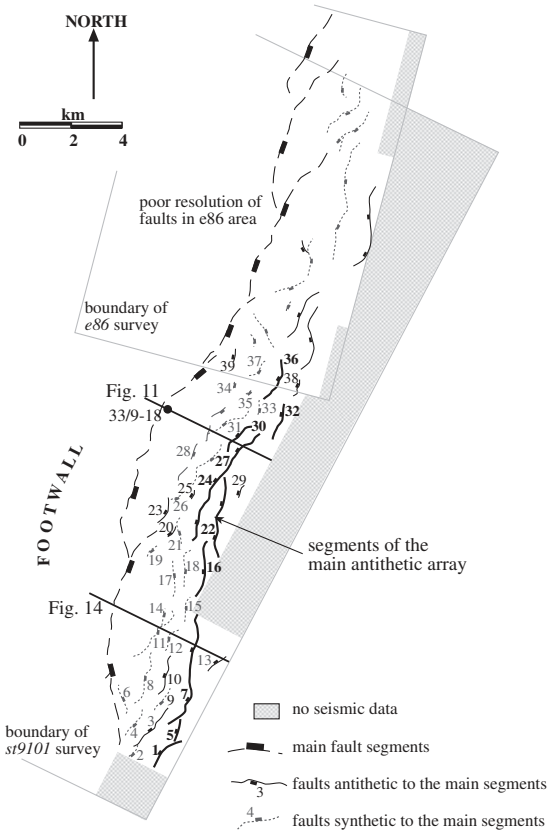

Figure 12: The population of normal faults mapped in the hangingwall of the Strathspey-Brent-Statfjord fault array. Traces of all faults are shown at the downthrown contact with the top pre-rift reflector (see Fig. 11). Faults are separated into sub-populations of those antithetic and those synthetic to the half-graben bounding fault. Also shown are the locations of seismic lines in Figs. 11 and 14.

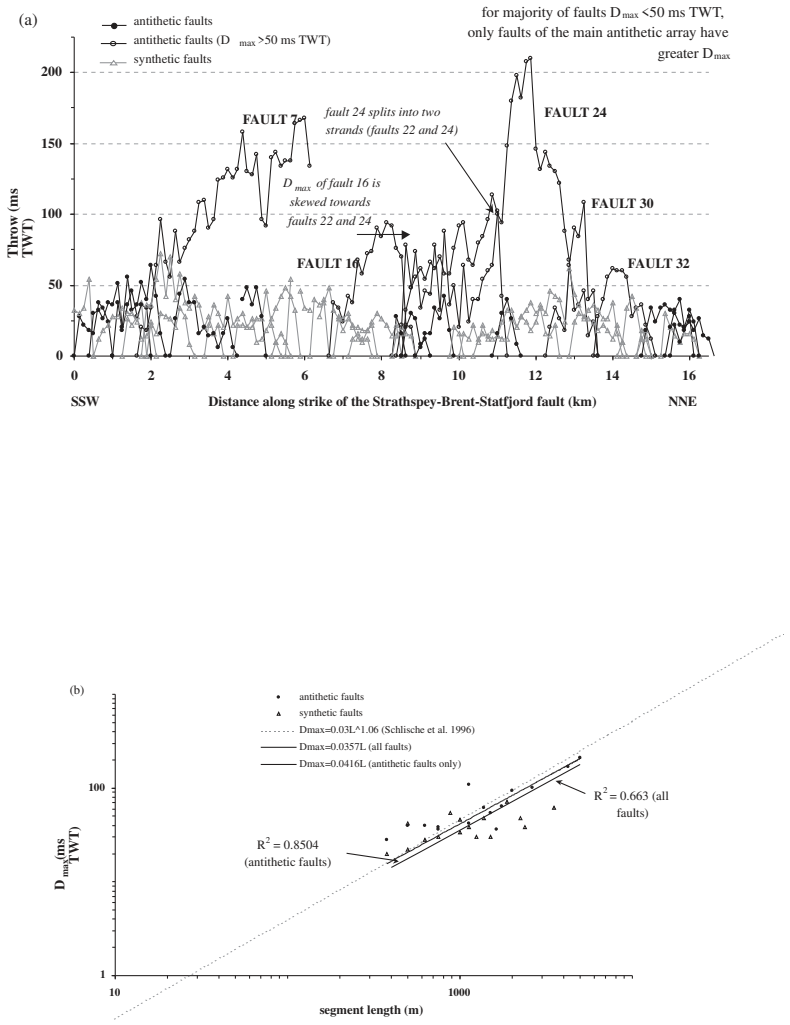

Figure 13: Faults in the hangingwall of the Strathspey-Brent-Statfjord fault array. (a) Displacement-distance profiles of a population of 39 faults (numbered on Fig. 12). The majority of these structures have a maximum displacement of <50 ms TWT. Faults 7, 16, 22, 24, 30 and 32 comprise the main antithetic array. (b) Plot of the segment length against the maximum displacement for the 39 faults in (a). Incomplete faults with tips outwith the coverage of the seismic data are excluded from this plot. Also shown is the displacement-length scaling relationship determined for the global dataset by Schlische et al. (1996). Note that the conversion of throw (in ms TWT) to displacement (in m) would increase values by approximately one third.

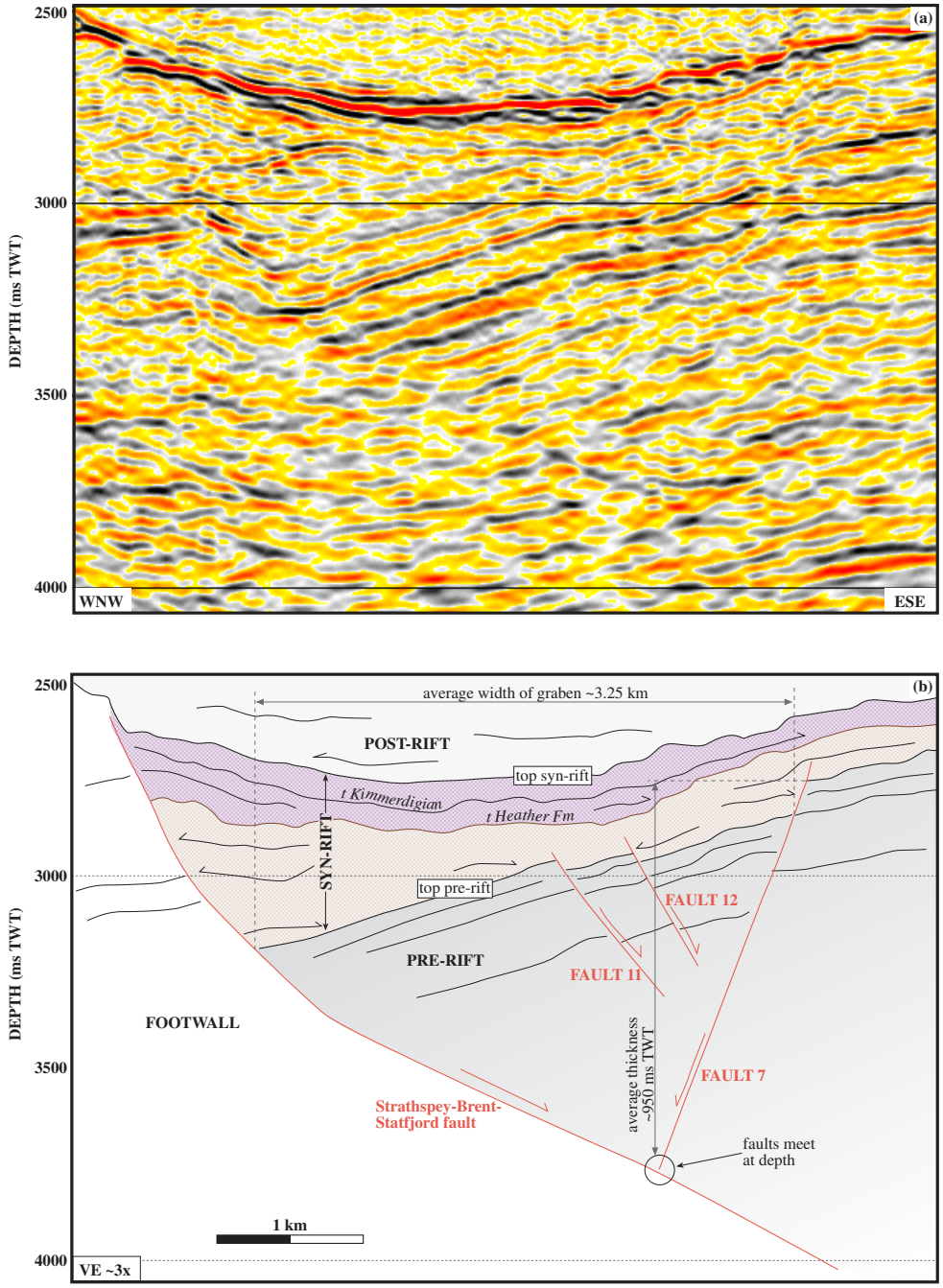

Figure 14: The architecture of the half-graben basin bounded by the Strathspey-Brent-Statfjord fault array. Faults in the hangingwall to the Strathspey-Brent-Statfjord fault system were only active during the initial 11.5 M.yr. of the rift history when the form of the basin was graben-like. (a) Seismic inline 390 from the Statfjord (st9101) survey; line is located on Fig. 12. (b) Interpretation of seismic line shown in (a). Vertical exaggeration is approximately three-fold.

6 Discussion

The Strathspey-Brent-Statfjord fault did not grow by simple radial propagation of a single fault segment but rather grew by the combined processes of tip propagation and segment linkage; hence, the throughgoing fault strand comprises a hierarchy of linked palaeo-segments. We have employed seismic mapping, seismic sequence stratigraphic techniques and fault scaling relationships to reconstruct the growth of the Strathspey-Brent-Statfjord fault array.

Our observations demonstrate that the half-graben bounding fault system is 'immature' (under-displaced) in terms of displacement-length scaling (Fig. 9). Although the entire fault is not covered by the available data, it is clearly much greater than 62 km in length. If the maximum displacement of c.2.3 km, observed 12.5 km from the southern margin of this study, is indeed the maximum displacement on the array, then (using the reasonable assumption that the maximum throw occurs near the centre of the fault) the predicted total length of the fault is approximately 100 km. The implication of this is that the fault bounding the Alwyn North hydrocarbon field is the southern extension of the Strathspey-Brent-Statfjord fault array (Fig. 1b). The observed maximum displacement of c.2.3 km is lower than would be predicted for a 100 km long fault using the displacement-length scaling relationship Dmax = 0.03L, see Schlische et al. (1996). In addition, significant variations in displacement are recorded along the strike of the fault - remnants of the displacement-distance profiles of the early, unlinked fault segments. The perceived immaturity of the Strathspey-Brent-Statfjord fault array is most likely to be due to the cessation of extensional tectonics before the fault grew to achieve a displacement-length relationship consistent with that of the observed global dataset. Consequently, the immature characteristics of the fault system provide an insight into the history of displacement accumulation.

A schematic reconstruction of the growth of the Strathspey-Brent-Statfjord fault array is presented in Fig. 15. This model is based on observations from the central part of the system, mainly from the Brent segment, between 10-30 km along-strike. From the displacement-distance profile (Fig. 10a) and the locations and ages of splay faults (abandoned fault tips; Fig. 7), five en echelon palaeo- fault segments of 3-7 km length are recognised in this section of the array. The three-stage reconstruction illustrates the growth of these five, initially isolated, segments to form a single, throughgoing fault strand with a displacement-distance profile comparable to that observed from the study area. The emphasis in this discussion is relative rates of displacement; thus for each stage the grey region on the displacement-distance profile is an indication of the relative rate of displacement along the array.

In stage 1 of the reconstruction (Fig. 15), five en echelon fault segments are observed. Although each segment comprises a linked array (evidenced by along-strike displacement variations), at this scale the segments can be considered relatively isolated; hence, displacement-distance profiles are symmetrical. In stage 1 faults 3, 4 and 5 remain isolated. The isolated segments grow by radial tip propagation, following the growth path Dmax = c.L^n, with maximum rates of displacement at the centre of the segments. Continued slip and the lateral propagation of neighbouring faults 1 and 2, however, leads to the interaction of stresses local to the structures (Bürgmann et al., 1994) (Willemse et al., 1996) (Willemse, 1997). This results in an increase in the rate of displacement on both segments, particularly in the region of fault overlap, e.g. Cowie (1998), Gupta and Scholz (2000). Consequently, the positions of maximum displacement on faults 1 and 2 are skewed from the centre of the strands towards the adjacent structure. In addition, the two faults are shown to accumulate displacement with little increase in strand length, i.e. although unlinked, the segments are beginning to behave as a single fault, cf. Dawers and Anders (1995).

Ultimately faults 1 and 2 'hard-link', the relay ramp is breached and the two segments join to form a single strand (stage 2, Fig. 15). Overlapping segment tips are now abandoned. With linkage the length of fault 1-2 increases whilst the maximum displacement is little changed; hence, the ratio of maximum displacement to length decreases significantly. Fault 1-2 in stage 2 is 'immature', with respect to displacement-length scaling and also the displacement minimum that defines the point of segment linkage. In the conceptual model of Cartwright et al. (1995), such immature characteristics are lost as the linked fault grows, i.e. the structure equilibrates back to a self-similar profile shape. This model requires extremely high displacement rates at the palaeo- segment boundary without lateral propagation at the tips. Observations from the Strathspey-Brent-Statfjord fault array, however, do not support this model but show that the along-strike displacement variations of palaeo-segments are largely preserved following linkage. The implication is that a simple model for the linkage of 2-3 segments in which along-strike displacement deficits are eradicated during subsequent fault growth may not be applicable to a complex multi-segment array.

In stage 2 of the reconstruction (Fig. 15), the northern tip of linked fault 1-2 approaches the southward propagating tip of the previously isolated fault 3. As a consequence, the highest rates of displacement accumulation on fault 1-2 are in the region of interaction with fault 3 and not at the palaeo- segment boundary. We consider the effects of fault interactions to be the primary control on the rate of displacement along the Strathspey-Brent-Statfjord fault array at

this time. In this reconstruction, the central displacement minimum on fault 1-2, marking the point of fault linkage, is preserved. Fault 3 develops a displacement-distance profile skewed towards fault 1-2 and a high ratio of maximum displacement to segment length (compared with that of an isolated fault). Faults 4 and 5 continue to grow in isolation.

In the final stage of the reconstruction shown, fault 1-2 and fault 3 are 'hard-linked'. The throughgoing fault 1-2-3 is interacting with fault 4, which, in turn, is interacting with fault 5. Interactions between the stresses local to individual segments are again suggested to be the primary control on rates of displacement accumulation along the array.

The stratal architecture of coeval syn-rift sediments dates the linkage of these five fault segments as Early - Middle Oxfordian (Fig. 7), 11-14 M.yr. after the initiation of rift tectonics. Subsequently, during the Late Oxfordian - Ryazanian (the next 18.5 M.yr.), this part of the Strathspey-Brent-Statfjord fault accumulated >1.25 km displacement (Fig. 9). This post-linkage displacement appears to have been relatively even along the central portion of the array without significantly affecting the magnitude of remnant displacement variations (Fig. 10b). The evolution of an overall flat-topped profile shape with a linear tip gradient would have occurred over numerous sub-strand length rupture events (Cowie and Shipton, 1998). The distribution of individual slip events along the array during this phase of the growth of the fault is, of course, unknown. The observations of this study, however, suggest that segment boundaries played an important role as sites of rupture nucleation or arrest only during the earliest stages of rifting, i.e. prior to and during, but not after, segment linkage. Further, it is proposed that this >>62 km long linked array effectively behaved as a single fault strand, with the potential for large rupture events, cf. Jackson and Blenkinsop (1997).

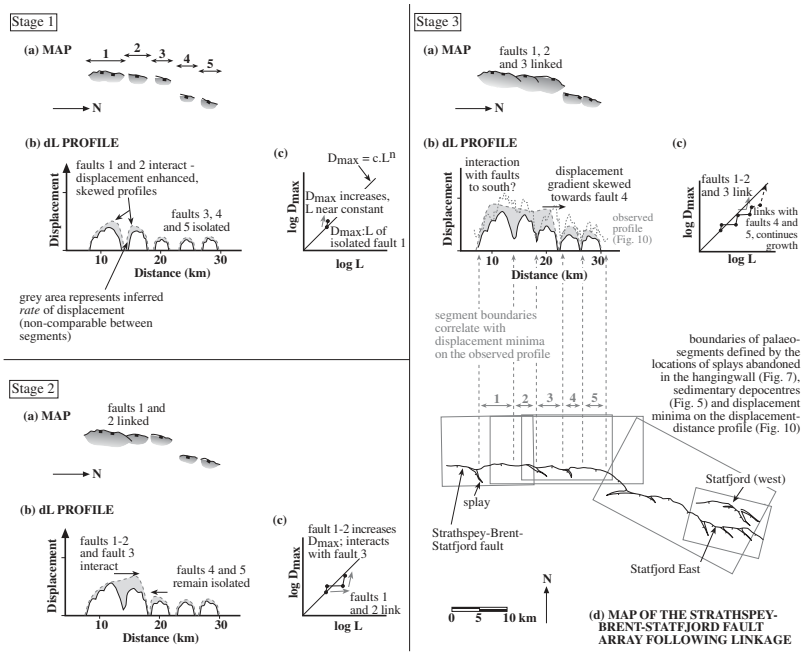

Figure 15: Schematic model of the growth of the Strathspey-Brent-Statfjord fault system. Based on the observations from the displacement-distance profile between 10-30 km along-strike (Fig. 10a). In each stage, (a) is a plan view of the fault system with depocentres shaded in grey, (b) is a schematic displacement-distance profile and (c) is a plot of Dmax against L for the evolving fault 1. See text for further explanation.

7 Conclusions

- Two sub-populations of Late Jurassic faults are described from the Strathspey-Brent-Statfjord area of the northern North Sea. We recognise a long-lived group of faults associated with the growth of the half-graben bounding Strathspey-Brent-Statfjord fault, and a second sub-population, located in the hangingwall to the main fault, that became inactive early in the rift event.

- The Strathspey-Brent-Statfjord fault is a single throughgoing strand of length >>62 km and maximum displacement of c.2.3 km. At 5-13 km spacing along this fault splay faults arc out into the hangingwall basin. The splay faults are interpreted as palaeo- fault tips abandoned in the hangingwall when two fault segments 'hard-linked'; hence, the Strathspey-Brent-Statfjord fault comprises a hierarchy of linked palaeo-segments. Stratigraphic evidence dates the majority of tip abandonment and linkage events as latest Callovian - Middle Oxfordian.

- Although an overall flat-topped profile shape is suggested, the displacement-distance profile of the Strathspey-Brent-Statfjord fault has significant along-strike variations in displacement. These variations are interpreted to represent preservation of the displacement-distance profiles of early unlinked fault segments. Examination of remnant displacement-length scaling relations of the palaeo-segments suggests little or no equilibration of local displacement variations following linkage.

- The sub-population of faults in the hangingwall of the Strathspey-Brent-Statfjord fault array is further divided into two groups. The first comprises both antithetic and synthetic faults of <3 km length and maximum displacements of up to 50 ms TWT. These faults were active during only the initial 3-4 M.yr. of the rift event. The second group of faults is an array of antithetic faults located c.3.5 km basinward of, and striking sub-parallel to, the half-graben bounding fault. These faults are linked arrays of up to 12 km length with maximum displacements typically <250 ms TWT; they became inactive after 11.5 M.yr.

- Early in the rift history a dense population of faults nucleated in the Strathspey-Brent-Statfjord area. Within 3-4 M.yr., however, the majority of these faults had become inactive and the basin evolved into a graben-like geometry. Approximately 11.5 M.yr. into the rift event, the array of faults bounding the eastern margin of the graben also became inactive, possibly due to the intersection of conjugate faults at depth. The basin subsequently developed a half-graben form bounded by the linked Strathspey-Brent-Statfjord fault. As the number of active faults decreased through the rift event, strain was localised on a few structures which subsequently experienced increased rates of fault displacement.

- We present a schematic reconstruction of the growth of the Strathspey-Brent-Statfjord fault array based mainly on observations from the Brent segment. In this reconstruction, interaction between neighbouring faults is considered to be the primary control on the rate of displacement accumulation along the array prior to and during segment linkage. We infer that, following linkage, ancient segment boundaries were not preferred sites of rupture nucleation or arrest.

8 Acknowledgments

This study was completed at the University of Edinburgh. We gratefully acknowledge Norsk Hydro, Shell/Esso, Statoil and Texaco (and their partners) for access to proprietary 3D seismic and well data. Tim Juett, Erik Lundin, Gunn Mangerud and Steve Taylor assisted in facilitating data release and financial support. This work benefited from discussions with Patience Cowie, Sarah Davies, Rob Gawthorpe, Ruth Gilpin, Bruce Trudgill and Jon Turner. Roy Schlische and Graham Yielding are thanked for thorough reviews of this manuscript.

The University of Edinburgh's seismic interpretation facilities, using Schlumberger GeoQuest IESX software, were funded by the Centre for Marine and Petroleum Technology, Norsk Hydro and Shell/Esso. Computing support at Edinburgh was provided by Chung-Lun Lau and James Jarvis. AEM was funded by a Natural Environment Research Council (NERC) Industrial CASE studentship with partners the Cambridge Arctic Shelf Program (CASP), Oryx (now Kerr McGee), Shell/Esso, Statoil and Texaco. NHD was funded by NERC under the Realising Our Potential Award scheme. JRU acknowledges Norsk Hydro for supporting his academic position during the period of this study.

References

M. H. Anders and R. W. Schlische. Overlapping faults, intrabasin highs and the growth of normal faults. *J. Geol.*, 102:165–180, 1994.

B. Armstrong. The temporal and spatial evolution of clastic syn-tectonic sedimentation on and adjacent to a developing relay ramp: An example from the Suez Rift. Master's thesis, The University of Edinburgh, 1997.

M. E. Badley, B. Freeman, A. M. Roberts, J. S. Thatcher, J. Walsh, J. Watterson, and G. Yielding. Fault interpretation during seismic interpretation and reservoir evaluation. In *The integration of geology, geophysics and petroleum engineering in reservoir delineation, description and management*, pages 224–241, 1990.

M. C. Budding and H. F. Inglin. *Petroleum geology of the continental shelf of northwest Europe*, chapter A reservoir geological model of the Brent sands in Southern Cormorant, pages 326–334. Heyden, London, 1981.

R. Bürgmann, D. D. Pollard, and S. J. Martel. Slip distributions on faults: effects of stress gradients, inelastic deformation, heterogeneous host-rock stiffness, and fault interaction. *J. Struct. Geol.*, 16:1675–1690, 1994.

J. A. Cartwright, B. D. Trudgill, and C. M. Mansfield. Fault growth by segment linkage: an explanation for scatter in maximum displacement and trace length data for the Canyonlands grabens of SE Utah. *J. Struct. Geol.*, 17:1319–1326, 1995.

C. Childs, J. Watterson, and J. S. Walsh. Fault overlap zones within developing normal fault systems. *J. Geol. Soc., Lond.*, 152:535–549, 1995.

J. Contreras, M. H. Anders, and C. H. Scholz. Growth of a normal fault system: Observations from the Lake Malawi basin of the east African rift. *J. Struct. Geol.*, 22:159–168, 2000.

J. Contreras, C. H. Scholz, and G. C. P. King. A model of rift basin evolution constrained by first-order stratigraphic observations. *J. Geophys. Res.*, 102:7673–7690, 1997.

P. A. Cowie. A healing-reloading feedback control on the growth rate of seismogenic faults. *J. Struct. Geol.*, 20:1075–1087, 1998.

P. A. Cowie and C. H. Scholz. Displacement-length scaling relationship for faults: data synthesis and discussion. *J. Struct. Geol.*, 14:1149–1156, 1992.

P. A. Cowie and Z. K. Shipton. Fault tip displacement gradients and process zone dimensions. *J. Struct. Geol.*, 20:938–998, 1998.

N. Dahl and T. Solli. *Petroleum Geology of Northwest Europe: Proceedings of the 4th Conference*, chapter The structural evolution of the Snorre Field and surrounding areas, pages 1159–1166. The Geological Society, London, 1993.

S. J. Davies, N. H. Dawers, A. E. McLeod, and J. R. Underhill. Controls on the spatial and temporal evolution of early syn-rift deposition: The Middle Jurassic Tarbert Formation, northern North Sea. *Basin Res.*, 12:343–365, 2000.

N. H. Dawers. *Observations of fault growth scaling relations.* PhD thesis, Columbia University, New York, 1997.

N. H. Dawers and M. H. Anders. Displacement-length scaling and fault linkage. *J. Struct. Geol.*, 17:604–614, 1995.

N. H. Dawers, M. H. Anders, and C. H. Scholz. Fault length and displacement: Scaling laws. *Geology*, 21: 1107–1110, 1993.

N. H. Dawers, A. M. Berge, K. O. Häger, C. Puigdefabregas, and J. R. Underhill. *Petroleum Geology of NW Europe: Proceedings of the 5th Conference*, chapter Controls on Late Jurassic, subtle sand distribution in the Tampen area, Northern North Sea, pages 827–838. The Geological Society, London, 1999.

N. H. Dawers and J. R. Underhill. The role of fault interaction and linkage in controlling syn-rift stratigraphic sequences: Late Jurassic, Statfjord East area, northern North Sea. *Bull. Am. Ass. Petrol. Geol.*, 84:45–64, 2000.

C. J. Ebinger, J. A. Jackson, A. N. Foster, and N. J. Hayward. Extensional basin geometry and the elastic lithosphere. *Phil. Trans. Roy. Soc. Lond. A*, 357:741–765, 1999.

R. L. Gawthorpe, A. J. Fraser, and R. E. Ll. Collier. Sequence stratigraphy in active extensional basins: Implications for the interpretation of ancient basin fills. *Mar. Petrol. Geol.*, 11:642–658, 1994.

F. M. Gradstein, F. P. Agterberg, J. G. Ogg, J. Hardenbol, P. Van Veen, J. Thierry, and Z. Huang. A Mesozoic time scale. *J. Geophys. Res.*, 99:24051–24074, 1994.

E. Graue, W. Helland-Hansen, J. R. Johnsen, L. Lømo, A. Nøttvedt, K. Ronning, A. Ryseth, and R. J. Steel. *Petroleum Geology of North West Europe*, chapter Advance and retreat of the Brent Delta system, pages 915–937. Graham and Trotman, London, 1987.

A. Gupta and C. H. Scholz. A model of normal fault interaction based on observations and theory. *J. Struct. Geol.*, 22:865–879, 2000.

S. Gupta, P. A. Cowie, N. H. Dawers, and J. R. Underhill. A mechanism to explain rift basin subsidence and stratigraphic patterns through fault array evolution. *Geology*, 26:595–598, 1998.

S. Gupta, J. R. Underhill, I. R. Sharp, and R. L. Gawthorpe. Role of fault interactions in controlling syn-rift sediment dispersal patterns: Miocene, Abu Alaqa Group, Suez Rift, Sinai, Egypt. *Basin Res.*, 11:167–189, 1999.

N. J. Hayward and C. Ebinger. Variations in the along-axis segmentation of the Afar Rift system. *Tectonics*, 15:244–257, 1996.

W. Helland-Hansen, M. Ashton, L. Lømo, and R. Steel. *Geology of the Brent Group*, volume 61 of *Spec. Pub. Geol. Soc., Lond.*, chapter Advance and retreat of the Brent delta: Recent contributions to the depositional model, pages 109–127. 1992.

J. Hesthammer and H. Fossen. Evolution and geometries of gravitational collapse structures with examples from the Statfjord Field, northern North Sea. *Mar. Petrol. Geol.*, 16:259–281, 1999.

J. Jackson and T. Blenkinsop. The Bilila-Mtakataka fault in Malawi: An active, 100 km long, normal fault segment in thick seismogenic crust. *Tectonics*, 16:137–150, 1997.

J. Jackson and D. McKenzie. The geometrical evolution of normal fault systems. *J. Struct. Geol.*, 5:471–482, 1983.

E. P. Johannessen, R. Mjøs, D. Renshaw, A. Dallard, and T. Jacobsen. *Sequence stratigraphy on the northwest European margin*, volume 5 of *Spec. Pub. NPF*, chapter Northern limit of the 'Brent delta' at the Tampen Spur: A sequence stratigraphic approach for sandstone prediction, pages 213–256. 1995.

J. J. Lambaise. *Lacustrine basin exploration: case studies and modern analogs*, volume 50 of *Mem. Am. Ass. Petrol. Geol.*, chapter A model for tectonic control of lacustrine stratigraphic sequences in continental rift basins, pages 265–276. 1990.

M. R. Leeder and R. L. Gawthorpe. *Continental extensional tectonics*, volume 28 of *Spec. Pub. Geol. Soc., Lond.*, chapter Sedimentary models for extensional tilt-block/half-graben basins, pages 139–152. 1987.

A. E. McLeod and J. R. Underhill. *Petroleum geology of northwest Europe: Proceedings of the 5th conference*, chapter Processes and products of footwall degradation, northern Brent Field, northern North Sea, pages 91–106. Geological Society, London, 1999.

A. E. McLeod, J. R. Underhill, S. J. Davies, and N. H. Dawers. The influence of fault array evolution on syn-rift sedimentation patterns in the Strathspey-Brent-Statfjord half-graben, northern North Sea. *Bull. Am. Ass. Petrol. Geol.*, in press.

B. C. Mitchner, D. A. Lawrence, M. A. Partington, M. J. B. Bowman, and J. Gluyas. *Geology of the Brent Group*, volume 61 of *Spec. Pub. Geol. Soc., Lond.*, chapter Brent Group: Sequence stratigraphy and regional implications, pages 45–80. 1992.

C. K. Morley. Patterns of displacement along large normal faults: Implications for basin evolution and fault propagation, based on examples from East Africa. *Bull. Am. Ass. Petrol. Geol.*, 83:613–634, 1999.

A. Nøttvedt, A. M. Berge, N. H. Dawers, R. B. Færseth, K. O. Häger, G. Mangerud, and C. Puigdefabregas. *Dynamics of the Norwegian Margin*, volume 167 of *Spec. Pub. Geol. Soc., Lond.*, chapter Syn-rift evolution and resulting play models in the Snorre-H area, northern North Sea, pages 179–218. 2000.

D. C. P. Peacock and D. J. Sanderson. Displacements, segment linkage and relay ramps in normal fault zones. *J. Struct. Geol.*, 13:721–733, 1991.

D. C. P. Peacock and D. J. Sanderson. Geometry and development of relay ramps in normal fault systems. *Bull. Am. Ass. Petrol. Geol.*, 78:147–165, 1994.

G. Pickering, D. C. P. Peacock, D. J. Sanderson, and J. M. Bull. Modeling tip zones to predict the throw and length characteristics of faults. *Bull. Am. Ass. Petrol. Geol.*, 81:82–99, 1997.

S. Prosser. *Tectonics and seismic sequence stratigraphy*, volume 71 of *Spec. Pub. Geol. Soc., Lond.*, chapter Rift-related linked depositional systems and their seismic expression, pages 35–66. 1993.

R. P. Rattey and A. B. Hayward. *Petroleum Geology of Northwest Europe: Proceedings of the 4th Conference*, chapter Sequence stratigraphy of a failed rift system: The Middle Jurassic to Early Cretaceous of the Central and Northern North Sea, pages 215–249. The Geological Society, London, 1993.

R. Ravnås, K. Bondevik, W. Helland-Hansen, L. Lømo, A. Ryseth, and R. J. Steel. Sedimentation history as an indicator of rift initiation and development: The Late Bajocian - Bathonian evolution of the Oseberg-Brage area, northern North Sea. *Norsk Geologisk Tidsskrift*, 77:205–232, 1997.

P. C. Richards, G. K. Lott, H. Johnson, R. W. O'B. Knox, and J. B. Riding. *Lithostratigraphic nomenclature of the UK North Sea*, chapter Jurassic of the central and northern North Sea, page 219. British Geological Society, Nottingham, 1993.

A. M. Roberts, G. Yielding, N. J. Kusznir, I. M. Walker, and D. Dorn-Lopez. *Petroleum Geology of Northwest Europe: Proceedings of the 4th Conference*, chapter Mesozoic extension in the North Sea: Constraints from flexural backstripping, forward modelling and fault populations, pages 1123–1136. The Geological Society, London, 1993.

S. Roberts and J. Jackson. *The geometry of normal faults*, volume 56 of *Spec. Pub. Geol. Soc., Lond.*, chapter Active normal faulting in central Greece: an overview, pages 125–142. 1991.

R. W. Schlische. Half-graben basin filling models: New constraints on continental extensional basin development. *Basin Res.*, 3:123–141, 1991.

R. W. Schlische. Geometry and origin of fault-related folds in extensional settings. *Bull. Am. Ass. Petrol. Geol.*, 79:1661–1678, 1995.

R. W. Schlische and M. H. Anders. *Reconstructing the history of Basin and Range extension using sedimentology and stratigraphy*, volume 303 of *Spec. Pap. Geol. Soc. Am.*, chapter Stratigraphic effects and tectonic implications of the growth of normal faults and extensional basins, pages 183–203. 1996.

R. W. Schlische and P. E. Olsen. Quantitative filling model for continental extensional basins with applications to early Mesozoic rifts of eastern North America. *J. Geol.*, 98:135–155, 1990.

R. W. Schlische, S. S. Young, and R. V. Ackermann. Geometry and scaling relations of a population of very small rift-related normal faults. *Geology*, 24:683–686, 1996.

C. Scholz and J. Contreras. Mechanics of continental rift architecture. *Geology*, 26:967=970, 1998.

R. J. Steel and A. Ryseth. *Tectonic events responsible for Britain's oil and gas reserves*, volume 55 of *Spec. Pub. Geol. Soc., Lond.*, chapter The Triassic - Early Jurassic succession in the northern North Sea: Megasequence stratigraphy and intra-Triassic tectonics, pages 139–168. 1990.

R. S. Stein and S. E. Barrientos. Planar high-angle faulting in the Basin and Range: geodetic analysis of the 1983 Borah Peak, Idaho earthquake. *J. Geophys. Res.*, 93:11355–11366, 1985.

B. D. Trudgill and J. A. Cartwright. Relay-ramp forms and normal fault linkages, Canyonlands National Park, Utah. *Bull. Am. Ass. Petrol. Geol.*, 106:1143–1157, 1994.

J. R. Underhill and M. A. Partington. *Siliciclastic sequence stratigraphy*, volume 58 of *Mem. Am. Ass. Petrol. Geol.*, chapter Use of genetic sequence stratigraphy in defining and determining a regional tectonic control on the 'Mid-Cimmerian Unconformity': Implications for North Sea basin development and the global sea-level chart, pages 449–484. 1994.

E. J. M. Willemse. Segmented normal faults: Correspondence between three-dimensional mechanical models and field data. *J. Geophys. Res.*, 102:675–692, 1997.

E. J. M. Willemse, D. D. Pollard, and A. Aydin. Three-dimensional analysis of slip distributions on normal fault arrays with consequences for fault scaling. *J. Struct. Geol.*, 18:295–310, 1996.

G. Yielding. Footwall uplift associated with Late Jurassic normal faulting in the northern North Sea. *J. Geol. Soc., Lond.*, 147:219–222, 1990.

G. Yielding, M. E. Badley, and A. M. Roberts. *Geology of the Brent Group*, volume 61 of *Spec. Pub. Geol. Soc., Lond.*, chapter The structural evolution of the Brent Province, pages 27–43. 1992.